Advances in Molten Slags, Fluxes, and Salts: Proceedings of The 10th International Conference on Molten Slags, Fluxes and Salts (MOLTEN16)
Edited by: Ramana G. Reddy, Pinakin Chaubal, P. Chris Pistorius, and Uday Pal
TMS (The Minerals, Metals & Materials Society), 2016

REDUCTION OF IRON OXIDES IN MOULD FLUXES WITH ADDITIONS OF $CaSi_2$

Min Wang[1,2], Rie Endo[1], Yoshinao Kobayashi[1], Zuoyong Dou[2] and Masahiro Susa[1]

[1] Tokyo Institute of Technology;
2-12-1, Ookayama, Meguro-ku; Tokyo, 152-8552, Japan
[2] Institute of Materials, China Academy of Engineering Physics;
No. 9, Huafengxincun, Jiangyou, Sichuan, 621908, China

Keywords: Mould flux, Iron oxide, Reduction, Calcium silicide.

Abstract

Iron oxides in mould fluxes enhance heat extraction from the molten steel to the mould due to energy absorption by d-d transitions of Fe^{2+} and re-emission. Thus, the existence of iron oxides is against mild cooling of molten steel. In this study, mould flux powders containing *ca* 2 mass% Fe_2O_3 were mixed with sufficient amounts of $CaSi_2$. The mixtures were contained in alumina crucibles and melted at 1673 K in Ar-H_2 atmosphere. The melts were poured into brass moulds to obtain glassy samples 5 mm thick. The Fe_2O_3 concentration was analysed by a scanning electron microscope with an energy dispersive spectrometer. The concentration decreased from *ca* 1.71 mass% to 0.49 mass% within 5 min and then settled down. Mass transfer of Fe_2O_3 is supposed to be the rate-controlling step at high temperature. The mass transfer coefficient has been calculated to be 1.8×10^{-3} cm·s^{-1}, which seems reasonable. Since crystallisation of mould flux enhance heat reflection from the molten steel to reduce heat transfer, crystallisation kinetics of mould fluxes has been investigated using the Avrami equation, which suggests that additions of reducing agents such as $CaSi_2$ suppress the crystallisation process. In addition, $CaSi_2$ additions result in a dramatic decrease in the total radiative heat flux across mould fluxes in glassy state and would be effective for mild cooling of molten steel.

Introduction

Continuous casting requires mild cooling of molten steel to prevent longitudinal surface cracking. The cooling rate of the steel can be controlled using mould flux which has an influence on the heat transfer from the steel shell to the casting mould. The heat transfer takes place mainly through two mechanisms, namely, conduction and radiation, which could be both reduced by crystallisation of mould flux[1-3]. The addition of iron oxides enhances the radiative heat transfer across the mould flux film due to corresponding changes in optical properties including reflectivities, transmissivity and absorptivities[4,5]. It is necessary to reduce iron oxides in mould flux to give it suitable optical properties for production of steel slabs with good surface quality.

In a previous study mould fluxes it was found that oxygen dissolved in molten iron is the primary oxygen source leading to the dissolution of iron oxides in mould flux, and suggested that additions of reducing agents would be efficient methods of reducing iron oxide concentrations in the final flux materials[6]. Previous studies on the reduction of iron oxides from slags at high temperatures have that carbon in the form of coke or graphite can reduce the iron oxide to

several mass percent in slags[7-9]. These studies have succeeded in providing a good understanding of the kinetics of iron oxide reduction by carbon and the control of foaming phenomena by addition of carbonaceous materials for iron smelting. Carbon particles are commonly mixed with mould flux powders to prevent oxidation of the steel surface. However, these particles are not able to easily dissolve into mould flux baths and are maintained as solids, which have much lower reduction rate of iron oxide than solute carbon[8]. The carbon reduction usually results in the formation of gaseous carbon monoxide and carbon dioxide which would form gas bubbles in mould fluxes. Thus, carbon does not seem to be a suitable reducing source for iron oxides.

Against this background, this study reconsiders reducing agents other than carbon materials for the reduction of iron oxides in mould flux and chooses calcium silicide. Calcium silicide is being used in mould flux to maintain the steel temperature by the exothermic reaction with iron oxides. Although Tsukaguchi *et al*[10,11] have studied exothermic powder containing CaSi and FeO, they have mainly focused on heat of calcium silicide combustion instead of iron oxide reduction. Consequently, this study aims to investigate the reducibility of calcium silicide for the reduction of iron oxides in mould flux at a low concentration level, and to evaluate the crystallisation and radiative heat transfer characteristics of the reduced fluxes.

Experimental

A synthetic mould flux (base mould flux) was employed with the nominal composition (in mass%): Al_2O_3+MgO=3.23, Na_2O+F=19.6, Fe_2O_3=2.0, and the basicity T.CaO/SiO_2=1.0, **Table 1** gives the respective reducing conditions of Exps. 1-3.

Table 1. Summary of experimental conditions

	Mould flux	Reducing agent		Ambient gas	Temperature / K	Holding time / s
		Sort	Mass%			
Exp. 1	Base mould flux	-	-	Ar-H_2	1673	300
Exp. 2		$CaSi_2$, Φ ~300μm	3.1	Ar, Ar-H_2	1673	240, 600, 1200
Exp. 3			1.0, 2.0, 3.1	Ar-H_2	1673	1800

In Exp. 1, base mould fluxes in powders were used without reducing agent and melted at 1673 K in a platinum crucible in Ar-H_2 gas mixture. In Exps. 2-3, mould flux was used after sufficiently mixing with $CaSi_2$ and the mixture was melted at 1673 K in an alumina crucibles for reducing reaction within a desired holding time. At the end of each experiment, the melt was rapidly poured into a brass mould to obtain a glassy sample 5 mm thick. Parts of glassy samples were annealed above their crystallisation temperatures determined by DSC: the detailed annealing conditions are shown in **Table 2**.

Table 2. Annealing conditions

Sample	Reducing condition	Temperature / K	Holding time / s
Anneal-1	Exp. 1-0 %, Ar-H_2, 5 min	950	1800
Anneal-2	Exp. 3-1.0% $CaSi_2$, Ar-H_2, 30 min		
Anneal-3	Exp. 2-2.0% $CaSi_2$, Ar, 30 min	973	1800
Anneal-4-1	Exp. 2-3.1% $CaSi_2$, Ar, 20 min		
Anneal-4-2	Exp. 2-3.1% $CaSi_2$, Ar, 20 min	973	5400

The surface morphologies and the compositions of each of the samples were analysed by SEM-EDS after Au coating and the valence of iron ion was analysed by XPS. The phases present in the annealed samples were determined by XRD using Co K_α radiation. The apparent reflectivity (R_a) and transmissivity (T_a) were measured for glassy samples at room temperature using a spectrophotometer with an integrating sphere covering the wavelength range 300-2600 nm.

Results

The base mould flux in the glassy state appears yellowish green due to strong spectral absorption caused by ferric iron ion Fe^{3+} at wavelengths below 500 nm[4,12]. The reduced samples are generally in black colour and opaque, possibly due to strong absorption by dispersion of metallic particles in the samples. Metallic particles were found above the inner wall of alumina crucibles and seemed to be rich in iron, which agglomerated and separated from the molten mould flux due to the significant density difference between iron (7.25 $g \cdot cm^{-3}$)[13] and mould flux (2.40 $g \cdot cm^{-3}$)[14].

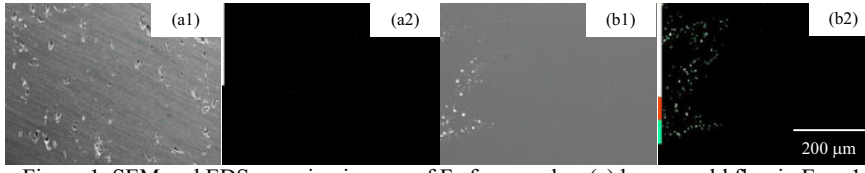

Figure 1. SEM and EDS mapping images of Fe for samples: (a) base mould flux in Exp. 1, and (b) a sample reduced by $CaSi_2$ in Exp. 2.

Figures 1(a)-(b) show SEM images and corresponding EDS mapping images of Fe for representative samples before and after reduction: (a) base mould flux, and (b) after $CaSi_2$ reduction. There is no sign corresponding to iron particles in the base mould flux, whereas iron rich particles in green colour are clearly observed in the sample with enough additions of $CaSi_2$ as shown in Fig. 1(b2). Corresponding EDS point analysis further proves low iron concentration areas in mould flux matrix and high iron concentration areas in iron rich particles. In addition, XPS profiles of Fe in the reduced sample have identified peaks at the binding energy around 707 and 711 eV corresponding to atomic Fe and Fe^{3+} ion[15]. The peak of atomic Fe agrees with the finding of iron rich particles by SEM-EDS. Thus, the concentration of iron oxide in the mould flux matrix has been calculated assuming that all iron oxide exists in the form of Fe_2O_3. The Fe_2O_3 concentration is *ca* 1.71 mass% in the base mould flux.

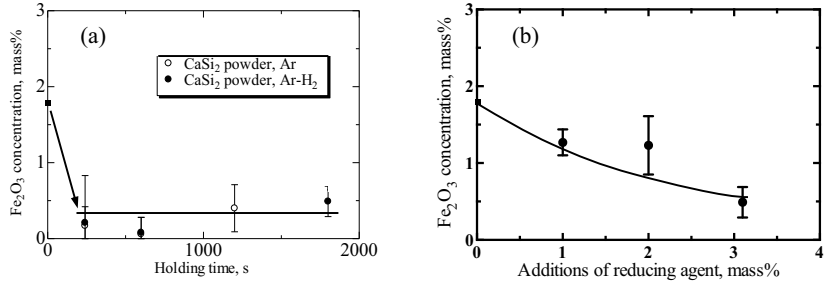

Figure 2. Fe_2O_3 concentration change with (a) holding time, and (b) $CaSi_2$ additions.

Figure 2(a) shows Fe_2O_3 concentration changes in mould fluxes by $CaSi_2$ reduction with holding time in Ar and Ar-H_2 atmosphere, respectively. Mould flux weighing 14 g empirically requires 2-3 min for complete melting. The reduction of iron oxide proceeds soon after melting of mould flux. There is almost no concentration dependence on atmosphere, which suggests that there is no influence of H_2 in atmosphere on iron oxide reduction. Figure 2(b) shows the iron oxide concentration change with $CaSi_2$ additions. The Fe_2O_3 concentration decreases to 0.49 mass% with additions of 3.1 mass% $CaSi_2$.

After annealing under the conditions described in Table 2, the base mould flux became milky white due to strong surface scattering. In contrast, the colour of reduced samples remains black with an almost imperceptible change. Small appearance differences of reduced samples before and after annealing give an indication of crystallisation. **Figures 3**(a) and (b) show SEM images of annealed samples corresponding to Anneal-4-1 and Anneal-4-2 conditions in Table 2. Crystallisation of grains in pale colour could be distinguished by inhomogeneous distribution in the observation field. Crystallisation is enhanced while the grains grow up with increasing holding time. Figure 3(c) shows a typical XRD profile of Anneal-4-2 sample. The identified peaks of cuspidine ($Ca_4Si_2O_7F_2$) is recognized as the crystalline phase.

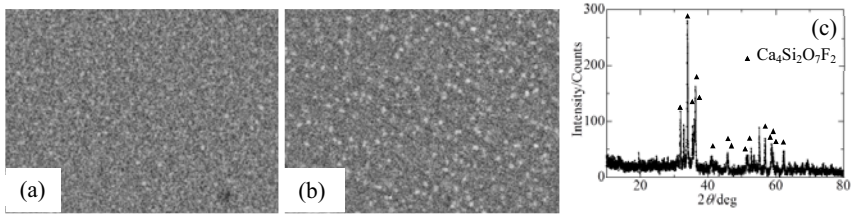

Figure 3. SEM images of (a) Anneal-4-1, and (b) Anneal-4-2 with (c) XRD profile for Anneal-4-2.

Figures 4(a), (b) and (c) show apparent transmissivities (T_a), reflectivities (R_a) and absorptivities (A_a) of glassy samples with and without $CaSi_2$ additions, respectively. For the base sample, the values of R_a remain at a low level over all wavelengths, while the values of A_a have absorption peaks below 500 nm and around 1000 nm due to ferric and ferrous iron ions. For the $CaSi_2$ reduced sample, there are low values of both R_a and T_a and high values of A_a probably due to the absorptions of metallic iron particles formed as a result of the reduction of Fe_2O_3 from the melt.

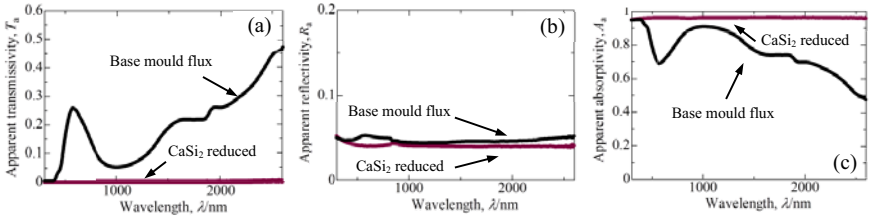

Figure 4. (a) Apparent transmissivities, (b) reflectivities and (c) absorptivities of samples.

Discussion

The reduction of Fe_2O_3 by $CaSi_2$ is assumed to follow Eq. (1):

$$Fe_2O_3\ (s) + \frac{3}{5}CaSi_2\ (l) = 2Fe\ (s) + \frac{3}{5}CaO\ (s) + \frac{6}{5}SiO_2\ (s) \quad (1)$$

Figure 2(a) has shown that the Fe_2O_3 concentration dramatically decreases with holding time and maintains constant after about 300 s. For high temperature redox reactions, the chemical reaction rate is commonly higher than the diffusion rate at high temperature. Therefore, mass transfer of Fe_2O_3 in the boundary layer is assumed to be the rate controlling step. The diffusion flux of Fe_2O_3 (J_{Fe2O3}) can be expressed by Eq. (2) following Fick's law.

$$J_{Fe_2O_3} = -\frac{D}{\delta} \cdot \left(C_{Fe_2O_3} - C^*_{Fe_2O_3}\right) = -k \cdot \left(C_{Fe_2O_3} - C^*_{Fe_2O_3}\right) \quad (2)$$

where δ is the boundary layer thickness, D is the diffusion coefficient of Fe_2O_3 in mould flux, k is the mass transfer coefficient of Fe_2O_3 across the boundary layer, C^*_{Fe2O3} is the equilibrium concentration of Fe_2O_3 and C_{Fe2O3} is the Fe_2O_3 concentration in mould flux. In addition, J_{Fe2O3} through the boundary layer per unit time can be expressed by Eq. (3) as well.

$$J_{Fe_2O_3} = \frac{V}{A} \cdot \frac{dC_{Fe_2O_3}}{dt} \quad (3)$$

where V is the volume of mould flux, A is the interfacial area and t is the holding time. By substituting Eq. (2) into Eq. (3) and integrating, the following equation can be derived and used to calculate the value of k.

$$\frac{V}{A} \cdot \ln\left(C_{Fe_2O_3} - C^*_{Fe_2O_3}\right) = -k \cdot t + \frac{V}{A} \cdot \ln\left(C^0_{Fe_2O_3} - C^*_{Fe_2O_3}\right) \quad (4)$$

where C^0_{Fe2O3} is the initial concentration of Fe_2O_3 in mould flux. Values of C_{Fe2O3} and C^0_{Fe2O3} in molar concentration have been derived from the mass fraction obtained by EDS analyses, molar mass and relevant densities (2.46 + 0.018×[C_{Fe2O3} in mass%] g/cm^3 for mould fluxes containing Fe_2O_3 around 1700 K[16], the value of C^*_{Fe2O3} at equilibrium is very low and assumed to be zero, the value of V has been calculated to be *ca* 12 cm^3 and the value of A has been estimated to be *ca* 36 cm^2. As a result, the value of k has been derived to be 1.8×10^{-3} cm·s^{-1}. This value for iron oxide reduction is much larger than the value for iron oxide formation[9] possibly due to larger interfacial areas for the reduction in powder mixture. In addition, it is suggested that iron oxide formation can be sufficiently suppressed by $CaSi_2$ within 600 s, which is as short as the estimated dwelling time of molten mould flux in continuous casting[9].

The crystallisation of mould flux has been investigated using the DSC profiles and the Avrami equation as follows:

$$\ln\{-\ln(1-x)\} = n \ln t + \ln K \quad (5)$$

where x is the relative degree of crystallinity, K is the crystallisation rate constant, t is the crystallisation time and n is the Avrami index[17-19]. At a start of crystallisation peak in the DSC profile, the time t is valued zero. While the time continuing, a corresponding value of x is calculated as the ratio of an instantaneous area over the whole area of the crystallisation peak in the DSC profile. The Avrami equation is a classic model applicable to explain crystallisation kinetics of materials including metal, ceramics and polymer on the assumptions: (i) nucleation occurs randomly and homogeneously in the entire untransformed portion of the material, (ii) growth occurs at the same rate in all directions, and (iii) the growth rate keeps constant.

Table 3 gives parameters of crystallisation kinetics including r, n, K, K_J and R^2 calculated using DSC curves, where r is the cooling rate of DSC analysis, K_J is the corrected constant of crystallisation rate satisfying the relationship $\ln K_J = \ln K / r$, and R is the correlation coefficient of the approximate curve. The value of R^2 entirely exceeds 0.95, which suggests that the Avrami equation is substantially applicable to explain the crystallisation kinetics of mould fluxes. Besides the sample reduced by $CaSi_2$ in this study, three other samples made previously have been compared[20-22]: the sample reduced by Si, base mould flux with *ca* 1.0 mass% Fe_2O_3 and

Fe_2O_3 free mould flux, respectively. The values of n for all four kinds of mould fluxes are around 3.0 in an agreement with Xie *et al*'s study[18,19], which indicates that cuspidine precipitates in the way of heterogeneous nucleation and has a 3-dimentional growth. The highest value of K_J for Fe_2O_3 free mould flux indicates a most rapid process of crystallisation. Crystallisation of mould flux is suppressed by the presence of iron oxide and reducing agents instead of enhancing the nucleation rate of cuspidine.

Table 3. Kinetics parameters of crystallisation on the basis of Avrami equation

	r, °C·min^{-1}	n	K	K_J	R^2
$CaSi_2$ reduced	10	2.8	0.0073	0.6114	0.9574
Si reduced[20)]	10	3.0	0.0160	0.6613	0.9971
Base mould flux[21)]	10	3.2	0.0127	0.6462	0.9564
Fe_2O_3 free mould flux[22)]	10	2.8	0.1373	0.8199	0.9712

The radiative heat flux across the reduced sample has been estimated by the following the optical process model previously established[20]. The key equation in the optical process model developed from the net radiation method is Eq. (6) for calculation of spectral radiative heat flux across the mould flux layer I_R:

$$I_R = \frac{\varepsilon_2}{1-\varepsilon_2}\left(\frac{N}{D} - E_{2-}\right) \tag{6}$$

where $N = [\varepsilon_4 E_{4-} + (1-\varepsilon_4)(\varepsilon_3 E_{3+} + R_a^* \varepsilon_3 E_{3-} + T_a^* \varepsilon_2 E_{2+})][1-(1-\varepsilon_1)R_a]$

$$+(1-\varepsilon_4)T_a[\varepsilon_1 E_{1+} + (1-\varepsilon_1)(\varepsilon_2 E_{2-} + R_a^* \varepsilon_2 E_{2+} + T_a^* \varepsilon_3 E_{3-})] \tag{7}$$

$$D = 1 - (2-\varepsilon_1-\varepsilon_4)R_a + (1-\varepsilon_1)(1-\varepsilon_4)(R_a^2 - T_a^2) \tag{8}$$

$$\text{and } E_j = 3.742 \times 10^{-16} n^2 \lambda^{-5} \left[\exp\left(\frac{1.439\times10^{-2}}{\lambda T_j}\right) - 1\right]^{-1} \tag{9}$$

where E_j is the blackbody radiation energy emitted at interface j, subscript "+" means the direction of the energy from the shell to the mould while "–" means the reverse direction, λ is the wavelength, n is the refractive index of materials refracting radiation, ε_1 (T_1) and ε_4 (T_4) are the respective emissivities (temperatures) of the shell and the mould, ε_2 (T_2) and ε_3 (T_3) are the respective emissivities (temperatures) of the solid flux at interfaces in contact with the liquid flux and the air gap layer, R_a and T_a are the respective apparent reflectivity and transmissivity of the solid flux, and R_a^* and T_a^* are the apparent reflectivity and transmissivity for radiation emitted within solid flux, respectively. Parameters involved take the following values: interfacial temperatures T_1 = 1800 K, T_2 = 1400 K, T_3 = 500 K, T_4 = 400 K, and the thickness of solid flux layer d_f = 5.0 mm. The total radiative heat flux ($I_{Total\ R}$) has been derived by integrating Eq. (6) for all wavelengths (0.3-10.0 μm in this study). The values of $I_{Total\ R}$ is *ca.* 9.05×10^4 and 464 W·m^{-2} for the base sample and the sample reduced by $CaSi_2$, respectively. Additions of $CaSi_2$ cause a decrease up to three orders of magnitude in radiative heat flux due to a large decrease in apparent transmissivities and an increase in apparent absorptivities as shown in Fig. 4. Although the crystallisation kinetics is slowed down, additions of $CaSi_2$ could cause a dramatic decrease in the total radiative heat flux across the glassy mould flux, which would be effective to realize mild cooling in actual continuous casting of steel.

Conclusions

Iron oxides in mould fluxes have been reduced by calcium silicide. Some of the reduced samples have been annealed for crystallisation.

- The average Fe_2O_3 concentration progressively decreases from *ca* 1.71 mass% to 0.49 mass% in mould fluxes with additions of $CaSi_2$ within 1.8 ks at a temperature of 1673 K.
- The apparent reaction rate constant for the reduction of iron oxide by $CaSi_2$ has been derived as the magnitude of 10^{-3} $cm \cdot s^{-1}$, which is much larger than for iron oxide formation: the addition of $CaSi_2$ is efficient to keep the iron oxide concentration at a low level.
- Crystallisation kinetics of mould fluxes has been investigated using the DSC profiles and the Avrami equation to suggest that crystallisation of mould flux is suppressed by the presence of iron oxide and $CaSi_2$ instead of enhancing the nucleation rate of cuspidine.
- Additions of $CaSi_2$ result in a dramatic decrease in the total radiative heat flux of mould fluxes in glassy state due to effects of metallic iron particles formed in the final flux materials and would be effective to realise mild cooling in actual continuous casting of steel.

References

1. K. Tsutsumi, T. Nagasaka and M. Hino, “Surface Roughness of Solidified Mold Flux in Continuous Casting Process,” *ISIJ Int.*, 39 (1999), 1150-1159.

2. H. Nakada, M. Susa, Y. Seko, M. Hayashi and K. Nagata, “Mechanism of Heat Transfer Reduction by Crystallization of Mold Flux for Continuous Casting,” *ISIJ Int.*, 48 (2008), 446-453.

3. M. Hanao, M. Kawamoto and A. Yamanaka, “Influence of Mold Flux on Initial Solidification of Hypo-Peritectic Steel in a Continuous Casting Mold,” *ISIJ Int.*, 52 (2012), 1310-1319.

4. M. Susa, A. Kushimoto, H. Toyota, M. Hayashi, R. Endo and Y. Kobayashi, “Effects of both crystallisation and iron oxides on the radiative heat transfer in mould fluxes,” *ISIJ Int.*, 49 (2009) 1722-1729.

5. Y. Kobayashi, R. Maehashi, R. Endo and M. Susa, “Effects of Valence Control of Iron Ions on Radiative Heat Transfer in Mould Flux,” *ISIJ Int.*, 53 (2013) 1725-1731.

6. M. Wang, Y. Kobayashi, R. Endo and M. Susa, “Formation Kinetics of Iron Oxide in Mould Flux during Continuous Casting,” *ISIJ Int.*, 53 (2013) 56-61.

7. H. Katayama, M. Matsuo, M. Yamauchi, M. Michitaka, T. Kawamura and T. Ibaraki, “Machanism of Iron Oxide Reduction and Heat Transfer Smelting Reduction Process with a Thick Layer of Slag,” *ISIJ Int.*, 32 (1992) 95-101.

8. P.K. Paramguru, H.S. Ray and P. Basu, “Some Kinetic Aspects of Reduction of FeO in Molten Slags by Solute Carbon,” *ISIJ Int.*, 37 (1997) 756-761.

9. A.K. Jouhari, R.K. Galgali, P. Chattopadhyay, R.C. Gupta and H.S. Ray, “Kinetics of Iron Oxide Reduction in Molten Slag,” *Scand. J. Metall.*, 30 (2001) 14-20.

10. Y. Tsukaguchi and M. Kawamoto: “Exothermic Mold Fluxes for Slab Casting in Sumitomo Metals” (Paper presented at the Proc. of 11th China-Japan Symp. on Iron ans Steel Tech., Beijing, 2007), 154.

11. Y. Tsukaguchi, S. Ura, A. Shiraishi, Y. Hitomi, T. Nagahata, “Development of Slab Casting Technology for High Carbon Steel” (Paper presented at the Proc. of 76th Steelmaking Conf., Warrendale, PA, 1993), 397.

12. M. Susa, K. Nagata and K. C. Mills, “Absorption Coefficients and Refractive Indices of Synthetic Glassy Slags Containing Transition Metal Oxides,” *Ironmaking Steelmaking*, 20 (1993) 372-378.

13. J. E. Jensen, W. A. Tuttle, R. B. Stewart, H. Brechna and A. G. Prodell: *BROOKHAVEN NATIONAL LABORATORY SELECTED CRYOGENIC DATA NOTEBOOK, VOLUME II* (Washington, D. C.: AUI 1980), XIV-E-2.

14. Verein Deutscher Eisenhüttenleute, *SLAG ATLAS 2nd ed.* (Düsseldorf: Verlag Stahleisen 1995), 316.

15. J. Chastain and R.K. King, Jr., *Handbook of X-ray Photoelectron Spectroscopy* (Chigasaki: ULVAC-PHI, Inc. 1995), 81.

16. Verein Deutscher Eisenhüttenleute, *SLAG ATLAS 2nd ed.* (Düsseldorf: Verlag Stahleisen 1995), 344.

17. M. Avrami, “Kinetics of Phase Change. II: Transformation-Time Relations foe Random Distribution of Nuclei,” *J. Chem. Phys.*, 8 (1940), 212-224.

18. B. Xie, Y. Lei, F. Qi and J. Diao, “Effects of MnO on non-isothermal crystallisation kinetics of mould fluxes using DSC curves” (Paper presented at the Technical Seminar of CC Mold Flux and Quality Control, Beijing, 2009), 72-84.

19. Y. Lei, B. Xie, F. Qi and J. Diao, “Effects of MnO on Crystallisation Kinetic Characteristics of Mould Fluxes,” *the Chinese Jounal of Process Engineering*, 8 (2008), 185.

20. M. Wang, R. Endo, Y. Kobayashi, Y. Susa and M. Susa, “Radiative Heat Transfer Reduction across Mould Fluxes with Silicon Additions as Reducing Agent for Continuous Casting of Steel,” *Taikabutsu Overseas*, 36 (2016).

21. R. Maehashi, “Effects of Valence Control of Iron Ions on Radiative Heat Transfer in Mould Flux” (in Japanese, bachelar thesis, Tokyo Institute of Technology, 2012).

22. A. Kushimoto, “Effect of Cuspidine Grain Sizes on Radiative Heat Transfer in Mould Fluxes” (in Japanese, master thesis, Tokyo Institute of Technology, 2011).